LANGMUIR

pubs.acs.org/Langmuir Article

High-Resolution Atomic Force Microscopy Investigation of Alginate Hydrogel Materials in Aqueous Media

Yunbo Zheng, Umit Celik, Charlotte Vorwald, J. Kent Leach, and Gang-yu Liu*

Cite This: *Langmuir* 2024, 40, 25631−25637 Read Online

ACCESS | Metrics & More | Article Recommendations

ABSTRACT: Alginate hydrogels are frequently used in 3D bioprinting and tissue repair and regeneration. Establishing the structure−property−performance correlation of these materials would benefit significantly from high-resolution structural characterization in aqueous environments from the molecular level to continuum. This study overcomes technical challenges and enables high-resolution atomic force microscopy (AFM) imaging of hydrated alginate hydrogels in aqueous media. By combining a new sample preparation protocol with extremely gentle tapping mode AFM imaging, we characterized the morphology and regional mechanical properties of the hydrated alginate. Upon cross-linking, basic units of these hydrogel materials consist of egg-box dimers, which assemble into long fibrils. These fibrils congregate and pile up, forming a sponge-like structure, whose pore size and distribution depend on the cross-linking conditions. At the exterior, surface tension impacts the piling of fibrils, leading to stripe-like features. These structural features contribute to local, regional, and macroscopic mechanics. The outcome provides new insights into its structural characteristics from nanometers to tens of micrometers, i.e., at the dimensions pertaining to biomaterial and hydrogel−cell interactions. Collectively, the results advance our knowledge of the structure and mechanics from the nanometer to continuum, facilitating advanced applications in hydrogel biomaterials.

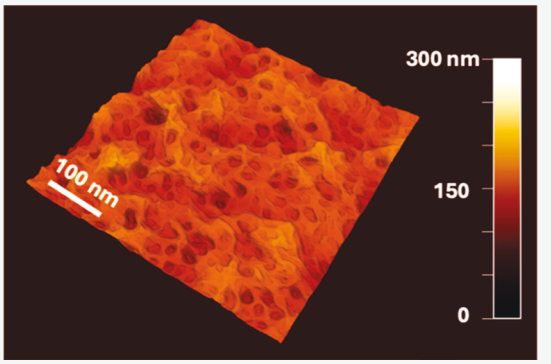

INTRODUCTION

Alginate hydrogel, consisting of natural linear polysaccharides composed of copolymeric blocks of (1−4)-linked β-D-mannuronic acid (M units) and α-L-guluronic acid (G units),[1] is frequently used in numerous biomaterial applications such as 3D bioprinting[2] and tissue engineering and regeneration[3,4] due to its high biocompatibility, high stability, ease of engineering, and ability to form stable gels in the presence of divalent cations such as calcium.[5−7] The hydrogel structure across dimensions, e.g., from nanometers to continuum, impacts its properties and performance in applications.[4,8−10] Prior work has revealed important insights pertaining to the hydrogel structure upon cross-linking. X-ray diffraction has revealed the basic unit in alginate hydrogel, known as egg-box dimer.[11,12] Microscopy techniques, such as scanning electron miscroscopy (SEM), cryo-SEM, and transmission electron microscopy (TEM) investigations also revealed fiber-like features at the exterior of the hydrogel materials.[13,14] However, there are limitations of the mesoscale structure characterization due to the drying and/or cryo-treatments of the hydrogel samples, which could alter the structure of the materials.[14−16] X-ray diffraction[11] and solid-state NMR spectroscopy[17] studies also indicated that the dehydration can significantly alter the alginate hydrogel structure. Therefore, there is an increasing need to characterize hydrogel materials in aqueous environment to reveal accurate structural information on the hydrated hydrogel and provide pertaining measurements of the structure and properties that cells "see and feel" for *in vitro* and *in vivo*. It is also important to attain both the exterior and interior structures of the hydrogel materials, which impacts the material performance.

Atomic force microscopy (AFM) is known to enable high-resolution imaging in physiological media and produce true 3D topographic information.[18,19] However, using AFM to image alginate hydrogel in aqueous media faced several technical challenges such as the "soft-and-sticky" nature of the materials, the movement of hydrogel thin films,[20] and AFM tips becoming blunt during scanning due to wearing or attachment of hydrogel materials. Thus, most AFM studies focused on imaging dried hydrogels under ambient conditions,[21,22] with a few exceptions that explored imaging in wet conditions, such as those with water droplets on the surface[23] or examining ultrathin alginate films[24] in aqueous media. To probe the alginate hydrogel material structure and properties in aqueous

Received: September 9, 2024
Revised: November 7, 2024
Accepted: November 8, 2024
Published: November 19, 2024

https://doi.org/10.1021/acs.langmuir.4c03554
Langmuir 2024, 40, 25631−25637

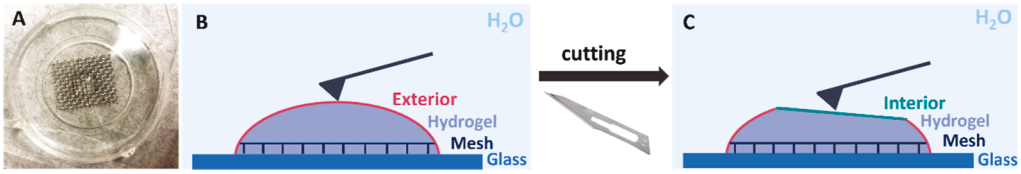

Figure 1. (A) A photograph shows a typical hydrogel sample prepared via our method described. (B) A schematic diagram illustrating AFM imaging of hydrogel exterior. (C) A schematic diagram illustrating AFM imaging of hydrogel interior after cutting the hydrogel in (B).

media, a new AFM imaging approach is necessary to allow imaging of hydrogel films with practical thickness. This work reports our method of sample preparation in conjunction with the extremely soft tapping mode AFM imaging. Both the exterior and interior of alginate hydrogels were investigated to reveal structural information from nanometers to the continuum. Regional mechanics[25−27] were also measured as a function of the degree of cross-linking, in correlation to the structural characterization. The information collectively provides a detailed view of alginate hydrogel structures across dimensions and in hydrated environments. The outcomes benefit the structure−property correlation and facilitate applications of alginate hydrogel materials in 3D biomaterial printing and tissue engineering and regeneration.

EXPERIMENTAL SECTION

Materials. Sodium alginate with a low viscosity (49.42 cP for 2% w/v concentration in water at 23 °C) and calcium chloride were purchased from Sigma-Aldrich (St. Louis, MO, U.S.A.). Ultrapure water with a resistivity of 18.2 MΩ·cm was produced from a Milli-Q water purification system (EMD Millipore, Billerica, MA, U.S.A.). MatTek glass-bottom dishes, P50G-1.5-30-F, were purchased from MatTek Corporation (Ashland, MA, USA).

Preparation of Alginate Hydrogel Samples. 2% (w/v) sodium alginate solution was obtained from dissolving in the Milli-Q water and stirring overnight. The viscosity of 2% sodium alginate was measured with a RheoSense microVISC viscometer at 23 °C. 130 μL of 2% (w/v) alginate aqueous solution was deposited to a stainless-steel mesh (1 mm periodicity) that was placed in the MatTek dish, immediately followed by adding $CaCl_2$ solution to it. After submerging the alginate in $CaCl_2$ for 2 h, the $CaCl_2$ solution was removed, and the hydrogel was rinsed with Milli-Q water. The MatTek dish was then refilled with Milli-Q water. The exterior hydrogel was characterized via AFM first, and then, a surgical blade (MedBlades, no. 11) was used to cut the hydrogel film and expose the interior of the hydrogel sample. A schematic diagram of the hydrogel sample preparation protocol is shown in Figure 1.

AFM Imaging of Alginate Hydrogel. All images were collected on an MFP-3D AFM (Oxford Instruments, Santa Barbara, CA, U.S.A.). Silicon cantilever (AC240TSA-R3, typical spring constant of 2.0 N/m, Olympus, Center Valley, PA, U.S.A.) was used to perform a light tapping mode in water. The scanning rates were usually 0.5−0.8 Hz. Each hydrogel sample was fully immersed in water during the entire AFM investigation. Image processing and analysis were conducted using MFP-3D software developed on the Igor Pro. 6.20 platform.

To ensure high-resolution imaging, we used fresh AFM tips under very gentle tapping conditions and closely monitored the image evolution with time. If tips became blunt, for example, due to wearing or hydrogel material attachment during the scan, we would stop the scan and switch to a fresh AFM probe.

The driving frequency was set to the natural resonance frequency of the cantilevers used, typically 21 kHz in water. The exterior area of alginate hydrogel was imaged via AFM first, with the damping set to be 4−10% of the 1 V free amplitude (~90 nm), i.e., the set point was 90−96% of the free amplitude. For AFM imaging of the interior, even lighter tapping was used with 1−2% damping of the 1 V free amplitude. This condition was selected to ensure gentle tapping and to avoid tip contamination.

Porosity Analysis. For hydrogel samples whose topographic images reveal pore features, we used ImageJ (NIH) to quantify the "coverage" of the pores. First, the AFM topographic image was imported into ImageJ and converted to a binary image. Next, the topographic image and the binary images were displayed side by side, and the threshold on the binary image was adjusted until the dark features replicated the pore features on the topographic images. Then, the depth of the shallowest pore was determined from the topographic image, serving as the standard for the assignment of pore features for all AFM images of hydrogels. Finally, the coverage of pore features can be directly read from the binary images by ImageJ.

Regional Mechanics Measurements via AFM. AFM indentation was done with the MFP-3D AFM using a modified AC240 cantilever. A 40 μm glass bead (Thermo Scientific, Fremont, CA) was glued with epoxy adhesive (Devcon, Glen View, IL) to the apex of the cantilever using our well-established method.[27,28] Briefly, the AFM tip was brought into contact with an epoxy glue line drawn on the glass surface to apply a small amount of glue. The glue-covered AFM tip was then positioned above a selected glass bead and contact was maintained for at least 30 min to ensure secure adhesion. The spring constant of the modified AFM tip was calculated using the added mass method,[29] which measured the resonant frequency before and after adding the glass bead. The spring constant was then calculated to be k = 2.0 N/m. The force-deformation was first acquired over a hard surface, in our case, a bare glass surface, from which deflection inverse optical lever sensitivity was determined, invOLs = 53.87 nm/V. This value was obtained by measuring the slope of the linear portion of the force curve when the cantilever was in contact with the glass surface. The probe was then positioned in proximity above the hydrogel surface, followed by acquiring force−distance profiles at the approaching/retracting speed of 2.0 μm/s. The maximum indentation depth was ~ 300 nm. Typically, force curves were obtained from six independent locations on the same hydrogel sample to ensure reproducibility and reliability. The Hertzian model[25,30,31] was used to fit the approach cycle of the curve to extract Young's modulus using the contact mechanical fits available in MFP-3D software, version AR 12. All measurements were carried out in water after collecting images on the areas of interest in the hydrogel. Poisson's ratio of 0.49 was used in the fitting for hydrated hydrogel.[32]

Statistical Analysis. Young's modulus values of the designated materials are reported as mean ± standard deviation. Each hydrogel sample included six replicates (n = 6).

RESULTS AND DISCUSSION

Preparing Hydrogel Materials for AFM Imaging in Aqueous Media. Alginate hydrogel materials were prepared using calcium ionic cross-linking of sodium alginate solution via immersion, following the commonly used method.[33] To address the aforementioned challenge of material movement, we placed a stainless-steel mesh (see Experimental Section) onto the surface support before depositing the hydrogel solution and performing cross-linking. The mesh served as a structural support to stabilize the hydrogel films on glass supports (Figure 1A). The exterior area (indicated by the red line in Figure 1B) was characterized via AFM first by positioning the probe above the top of the material. Then,

https://doi.org/10.1021/acs.langmuir.4c03554
Langmuir 2024, 40, 25631−25637

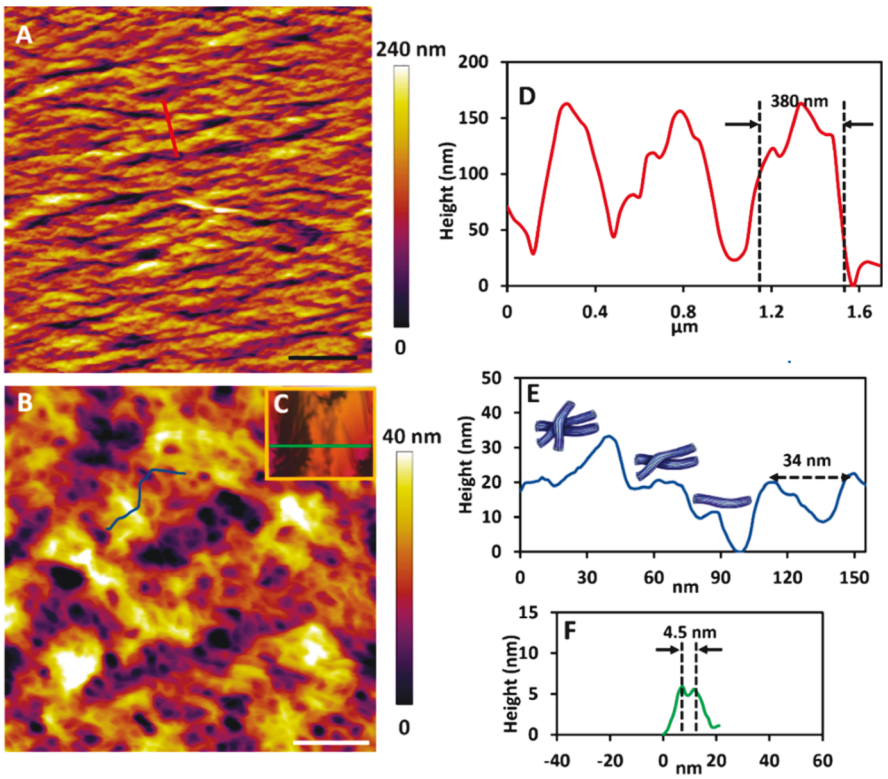

Figure 2. AFM imaging of alginate hydrogel cross-linked with 200 mM $CaCl_2$ for 2 h. (A) A representative topographic image from the exterior. Scale bar = 2 μm. (B) A zoom-in view of the hydrogel exterior. Scale bar = 100 nm. (C) A 3D and zoom-in view (22 nm × 18 nm) of an area containing two nearest neighbor fibrils. (D) Height profile of the red cursor indicated in image (A) and (E) height profile of the blue cursor indicated in image (B). The schematics above the peaks illustrate how the fibrils might pile. (F) Height profile of the green cursor indicated in image (C).

the interior area (indicated by the green line in Figure 1C) was exposed by cutting the hydrogel film with a surgical blade, immediately followed by AFM imaging. AFM force-deformation profiles were also acquired on both the exterior and interior to probe the regional mechanical properties. This method enabled high-resolution AFM imaging and measurements of regional mechanics in aqueous media.

High-Resolution Imaging of the Exterior of Alginate Hydrogel. The cross-linked hydrogel sample is approximately 5 mm wide and 2 mm tall. At least three different locations from the top surface were imaged to check for reproducibility. Figure 2A presents a representative 10 μm × 10 μm view of the exterior alginate upon soaking in 200 mM $CaCl_2$ solution for 2 h. This concentration was selected because it is commonly used in the preparation of alginate hydrogels for various biomedical applications.[34−36] The initial imaging area was determined using the lateral dimensions of typical MSC cells (15−30 μm) as a guide, to gain insights into what a cell may "see and feel" overall.[37,38] The AFM topography (Figure 2A) shows bright stripes extending across the scanned region. These stripes exhibit similar orientations and are separated by darker contrast in-between. The height profile as shown in Figure 2D across three representative stripes as shown in Figure 2A allows for quantification, e.g., the full width at half-maximum (fwhm) of 240, 340, and 380 nm and apparent height of 157, 152, and 158 nm, respectively. Considering all stripes in Figure 2A, the fwhm ranges from 130 to 850 nm.

A zoomed-in view (500 nm × 500 nm, Figure 2B) reveals the hydrogel structure within a typical stripe. At this scale, the structure of alginate hydrogel displays a Swiss-cheese-like morphology, with the crater features (dark contrast) surrounded by the piling of bright fibril features. For example, the height profile in Figure 2E shows a 34 nm wide crater. Those crater features measured in Figure 2B typically have openings ranging from 16 to 60 nm. The fibrils in Figure 2B were observed to bundle and pile, typically 8−17 nm in fwhm width and 3−17 nm in apparent height. The degree of fibril piling varies, as shown in the three examples in Figure 2E, with heights measured from 11 to 21 nm to 35 nm, respectively. The resolution of Figure 2B reached 4.5 nm, as demonstrated by the two clearly resolved nearest neighbor features shown in Figure 2C and the height profile in Figure 2F.

To the best of our knowledge, this is the first time that thick alginate hydrogel films were successfully imaged in aqueous media by using AFM with nanometer resolution. Our high-resolution AFM images provide structural information for the alginate hydrogel from the nanometer level to the mesoscale and beyond. Fiber X-ray diffraction has revealed that the basic unit in cross-linked alginate is "egg-box" dimer with a width of 0.86 nm.[12] Further association among these dimers could occur with the addition of cations into individual fibrils, which is referred to as bundling.[12,39,40] Our work enables visualization and measurement of these fibrils and their further assemblies, such as lateral association and/or piling up. In the case of hydrogel exterior, e.g., in Figure 2B, these fibrils assembled and piled up to form a "Swiss cheese" morphology within each stripe. The formation of stripes is unique to the exterior, likely due to the association of the fibril bundles under interfacial tension. With the updated knowledge in this AFM investigation, the structural description from molecular to

https://doi.org/10.1021/acs.langmuir.4c03554
Langmuir 2024, 40, 25631−25637

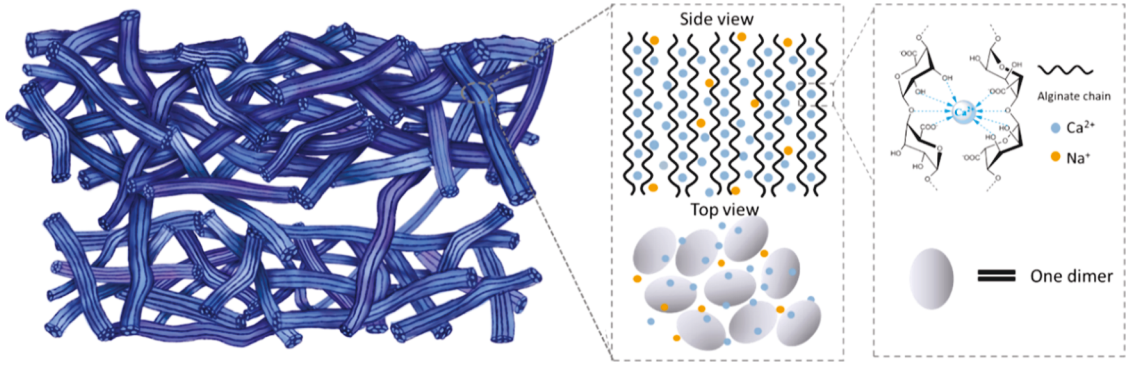

Figure 3. Schematic diagram illustrating the structure of the exterior of alginate hydrogel upon cross-linking. Right: the molecular structure of one "egg-box" dimer. Middle: dimer association to form fibrils (side and top views). Left: bundled and piled fibrils contributing to the observed Swiss-cheese morphology within each stripe, with two neighboring stripes displayed to reveal their alignment and separation.

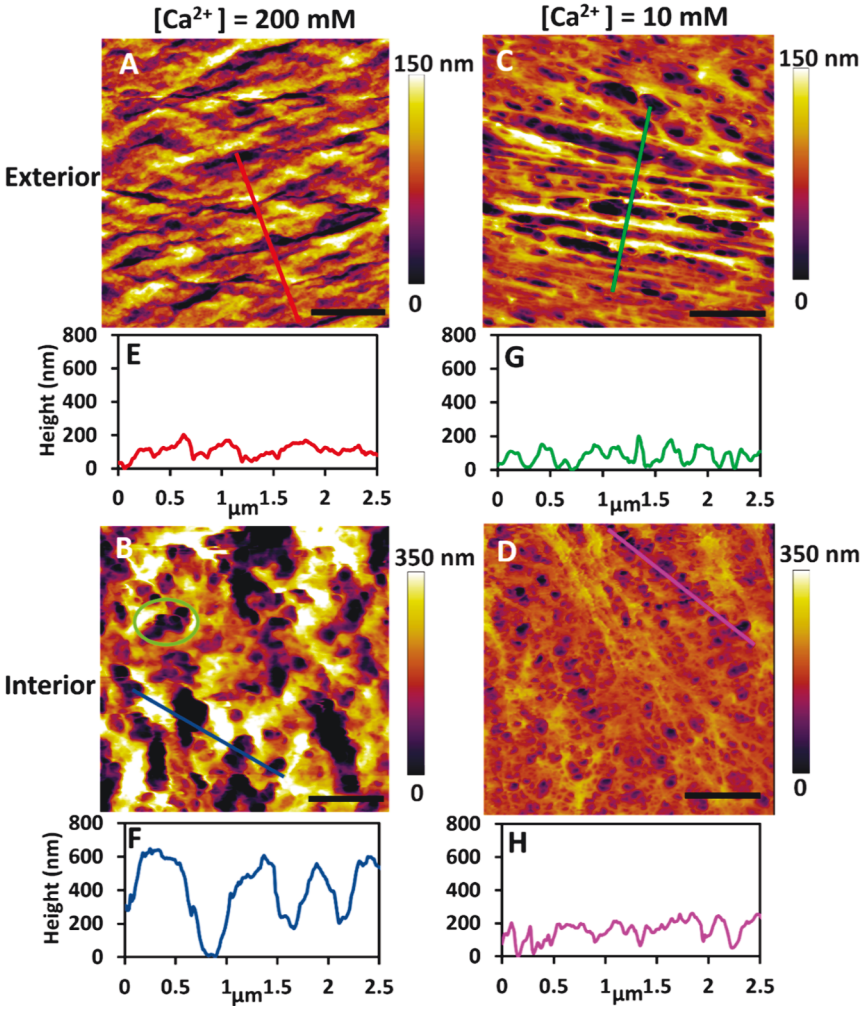

Figure 4. AFM topographic images and cursor profiles of alginate hydrogel cross-linked for 2 h via $CaCl_2$ solution with designed concentrations. (A) Exterior and (B) interior of alginate cross-linked with 200 mM $CaCl_2$. In (B), a green circle enclosed a complex pore, i.e., a large pore with 5 smaller pores within. (C) Exterior and (D) interior of alginate cross-linked with 10 mM $CaCl_2$. (E–H) Height profiles corresponding to the cursors shown in (A–D), respectively. Scale bars = 1 μm.

continuum for the hydrogel exterior is illustrated in the schematic diagram in Figure 3.

High-Resolution AFM Imaging of Alginate Hydrogel Interior. Our high-resolution AFM imaging of the alginate hydrogel's interior revealed significant structural differences from the exterior. Representative topographic images of the exterior and interior are displayed side by side in Figure 4. In contrast to the exterior discussed in the previous section and shown in Figure 4A, the interior presents a spongy-like structure (Figure 4B), characterized by dark pores surrounded by bright features. Many of these pores, e.g., indicated within the enclosure in Figure 4B, contain smaller pores embedded

https://doi.org/10.1021/acs.langmuir.4c03554
Langmuir 2024, 40, 25631−25637

within. The majority of these pores observed in Figure 4B have lateral dimensions of 150−300 nm, and their apparent depth ranges from 170 to 680 nm. For small pores, the depth likely represents an underestimation of the pore depth, as the AFM probe apex may be unable to reach the bottom. Overall, the interior exhibits a rougher morphology with a root-mean-square roughness of 128 nm compared to that of the exterior (34 nm). This local and nanoscale structural information is important for understanding cell−hydrogel interactions, as the size of the filopodia of cells fall into the pore size range.[41] Additionally, the pore structure could also impact the material mechanics, as discussed later in this work.

In correlation with the structural characterization, the regional mechanics of alginate were also measured using a 40 μm sphere attached to a microcantilever. Figure 5 shows a

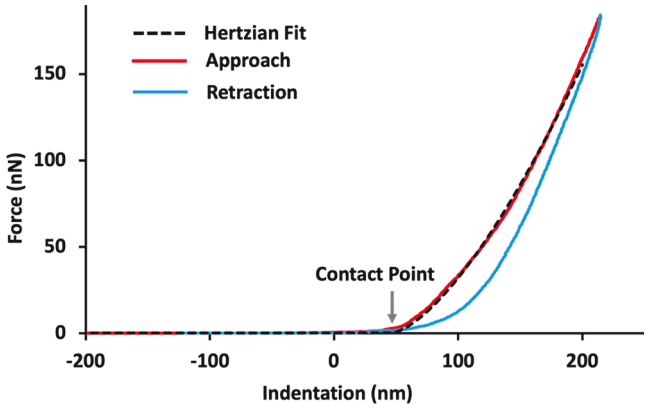

Figure 5. A representative force-deformation profile of the hydrogel shown in Figure 2, with the approach and retraction represented by red and blue lines, respectively. The fit using Hertzian mechanics is shown by the black dashed line. The arrow indicates the tip−surface contact point.

representative force-deformation profile taken on the exterior alginate cross-linked with 200 mM $CaCl_2$ in both approach and retraction cycle. There is little adhesion, as shown in Figure 5. The approach cycle is fitted with the Hertzian model,[25,30,31] yielding Young's modulus of 329 kPa. The fitting quality, indicated by the coefficient of determination R^2 = 0.999, demonstrates that the model works well with the experimental data. Young's moduli extracted for all hydrogel systems are summarized in Table 1, column 3. The interior of hydrogel

Table 1. Young's Modulus of Hydrogel Samples Measured Using AFM-Based Regional Mechanics (n = 6)

cross-linking condition (Ca^{2+} concentration)	hydrogel region	Young's modulus (kPa)
200 mM	exterior	290 ± 90
200 mM	interior	23 ± 8
10 mM	exterior	16 ± 6
10 mM	interior	3 ± 1

exhibits Young's modulus of 23 ± 8 kPa (row 2 and column 3), indicating that the interior is softer than the exterior, with a modulus of 290 ± 90 kPa (row 1 and column 3).

While past spectroscopy studies (micrometer resolution) have indicated differences from the exterior to the interior of the alginate prepared by similar protocols to ours,[42,43] this work enables direct visualization of the structural differences in aqueous media and with nanometer spatial precision. These structural differences were rationalized by Ca^{2+} diffusion from external inward, causing a decrease in the degree of cross-linking.[44−46] The high-resolution imaging clearly reveals the structural manifestation of these differences, including Swiss cheese versus sponge morphology and differences in fibril assembly and piling within these features. These structural differences correlate well with the regional mechanical properties measured by modified AFM probes. Collectively, this work enables correlation between structure and regional mechanics, which are known to impact cellular behavior.[3,9] Variations in local mechanical properties influence stem cell differentiation, with softer regions supporting softer tissue development, such as cartilage, while stiffer regions promote osteogenic differentiation and bone formation.[9]

Impact of Calcium Ion Concentration. Under the same reaction time of 2 h, reducing $[Ca^{2+}]$ to 10 mM led to distinct morphological differences in both interior and exterior compared to that under 200 mM. The exterior cross-linked with 10 mM $CaCl_2$ (Figure 4C) is dominated by a large number of fibrils with smaller diameters compared to those observed under a higher concentration shown in Figure 4A. The degree of lateral association between fibrils is also reduced. The lateral dimensions of these features observed in Figure 4C, as measured by the height profile shown in Figure 4G, range from 60 to 180 nm, which is significantly smaller than that shown in Figure 4E (170 to 570 nm). The regional elasticity measurements reveal that the exterior formed at 10 mM appears softer, with Young's modulus of 16 ± 6 kPa, compared to that under 200 mM (290 ± 90 kPa).

The interior alginate after reaction with 10 mM $CaCl_2$ (Figure 4D) exhibited a different morphology from that at 200 mM, characterized by a large population of small pores with an apparent depth of 75−180 nm and fwhm of 98−170 nm. At 200 mM (Figure 4B), in comparison, the apparent depth measures 170−680 nm and fwhm ranges from 150 to 400 nm. To quantify pore coverage, the shallowest pore depth determined from the interior alginate cross-linked with 10 mM $CaCl_2$ (Figure 4D), approximately 44 nm, was used as a threshold in ImageJ for generating pore maps across all AFM images. The overall coverage (area %) and distribution of pores are more clearly visualized using our pore mapping, as shown in Figure 6, where dark and bright contrasts correspond to pore and fibril assembly regions, respectively. At 10 mM, the areal coverage of pores measures 46.9%, which is larger than that under 200 mM (37.6%). The coverage and distribution of sponge frames, i.e., fibril assemblies (bright contrast), are also

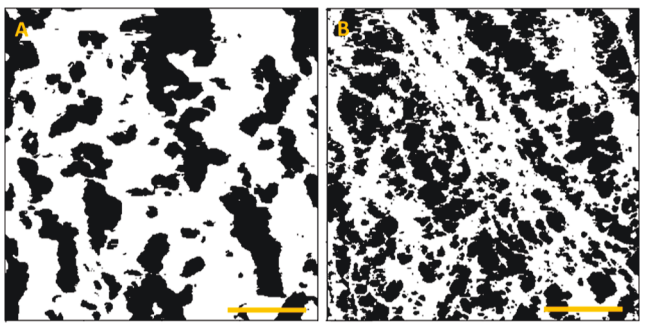

Figure 6. Pore maps generated from AFM topographic images of Figure 4B,D. (A,B) correspond to $[Ca^{2+}]$ at 200 and 10 mM, respectively. Scale bars = 1 μm.

https://doi.org/10.1021/acs.langmuir.4c03554
Langmuir 2024, 40, 25631−25637

clearly visible, with larger frames and higher coverage in the case of 200 mM than that under 10 mM. These detailed sponge structures provide the structural basis for the mechanical properties, e.g., Young's modulus measures 3 ± 1 kPa at 10 mM, which means softer than that at 200 mM (23 ± 8 kPa).

These observations are consistent with the explanation of a lower degree of cross-linking with decreasing [Ca^{2+}]. Similar trends were also reported in prior work using rheological measurements and tensile strength measurements, representing the bulk materials properties.[47,48] The new insights revealed in this investigation are the structural basis, from nanometer to macrolevel, that leads to the mechanical properties. At the nano- to microscale, we observed smaller fibrils and less bundling and piling among fibrils at lower [Ca^{2+}]. Regional Young's modulus is also smaller in both the interior and exterior of the hydrogel at a lower degree of cross-linking.

CONCLUSIONS

This work presents a high-resolution structural characterization of alginate hydrogels in aqueous media using AFM, by overcoming technical challenges of AFM imaging of soft-and-sticky materials. Our sample preparation protocols in conjunction with extremely soft tapping enable high-resolution imaging of the morphology and measurement of the regional mechanical properties. Upon cross-linking, the basic units of these hydrogel materials consist of egg-box dimers, which assemble into fibrils and fibril bundles. The final hydrogel materials are the outcomes of the assembly and piling of these bundles, manifesting into sponge-like structures at the interior. Cross-linking conditions, such as [Ca^{2+}], soaking time, and temperature, impact the bundle size and piling of bundles, which in turn influence the pore size and distribution as well as the sponge framework. At the exterior of the hydrogels, surface or interfacial tension comes into play, causing the fibrils to form stripe-like features. These new insights provide the structural basis for the observed mechanical properties at the local, regional, and macro levels. Work is in progress to investigate the impacts on hydrogel−cell interactions with the knowledge of structures from nanometers to tens of micrometers. The advancement of our understanding of the structure and mechanics from the nanometer scale to the continuum will facilitate applications in biomaterials, including tissue engineering and regenerative medicine.

AUTHOR INFORMATION

Corresponding Author

Gang-yu Liu − *Department of Chemistry, University of California, Davis, California 95616, United States;* orcid.org/0000-0003-3689-0685; Phone: (530) 754-9678; Email: gyliu@ucdavis.edu; Fax: (530) 752-8995

Authors

Yunbo Zheng − *Department of Chemistry, University of California, Davis, California 95616, United States*

Umit Celik − *Department of Chemistry, University of California, Davis, California 95616, United States*

Charlotte Vorwald − *Department of Biomedical Engineering, University of California, Davis, California 95616, United States*

J. Kent Leach − *Department of Biomedical Engineering, University of California, Davis, California 95616, United States; Department of Orthopaedic Surgery, UC Davis Health, Sacramento, California 95817, United States;* orcid.org/0000-0002-1673-3335

Complete contact information is available at: https://pubs.acs.org/10.1021/acs.langmuir.4c03554

Author Contributions

The manuscript was written through contributions of all authors. All authors have given approval to the final version of the manuscript.

Notes

The authors declare no competing financial interest.

ACKNOWLEDGMENTS

We thank Dr. Arpad Karsai, Andres Morales Maldonado, and Emma Lawrence at U.C. Davis for their technical assistance. We also thank Susan Stagner and Noah Haughn for careful proofreading. Helpful discussion with Drs. Roland Faller, Yuqi Huang, and Saswati Panda are appreciated. Financial support from the National Science Foundation (CHE-2304986), the National Institutes of Health (R01 AR079211), and the NHLBI Training Program in Basic and Translational Cardiovascular Science (T32 HL086350) are greatly appreciated. This publication is based upon work supported by (while the corresponding author serving at) the National Science Foundation.

REFERENCES

(1) Abka-Khajouei, R.; Tounsi, L.; Shahabi, N.; Patel, A. K.; Abdelkafi, S.; Michaud, P. Structures, properties and applications of alginates. *Marine Drugs* **2022**, *20* (6), 364.

(2) Axpe, E.; Oyen, M. L. Applications of alginate-based bioinks in 3D bioprinting. *Int. J. Mol. Sci.* **2016**, *17* (12), 1976.

(3) Alsberg, E.; Anderson, K.; Albeiruti, A.; Franceschi, R.; Mooney, D. Cell-interactive alginate hydrogels for bone tissue engineering. *J. Dent. Res.* **2001**, *80* (11), 2025−2029.

(4) Lee, J.-H.; Kim, H.-W. Emerging properties of hydrogels in tissue engineering. *J. Tissue Eng.* **2018**, *9*, 2041731418768285.

(5) de Vos, P.; Lazarjani, H. A.; Poncelet, D.; Faas, M. M. Polymers in cell encapsulation from an enveloped cell perspective. *Adv. Drug Deliv. Rev.* **2014**, *67*−*68*, 15−34.

(6) Drury, J. L.; Mooney, D. J. Hydrogels for tissue engineering: scaffold design variables and applications. *Biomaterials* **2003**, *24* (24), 4337−4351.

(7) Kuo, C. K.; Ma, P. X. Ionically crosslinked alginate hydrogels as scaffolds for tissue engineering: Part 1. Structure, gelation rate and mechanical properties. *Biomaterials* **2001**, *22* (6), 511−521.

(8) Caliari, S. R.; Burdick, J. A. A practical guide to hydrogels for cell culture. *Nat. Methods* **2016**, *13* (5), 405−414.

(9) Foster, A. A.; Marquardt, L. M.; Heilshorn, S. C. The diverse roles of hydrogel mechanics in injectable stem cell transplantation. *Current Opinion Chem. Eng.* **2017**, *15*, 15−23.

(10) Banerjee, A.; Arha, M.; Choudhary, S.; Ashton, R. S.; Bhatia, S. R.; Schaffer, D. V.; Kane, R. S. The influence of hydrogel modulus on the proliferation and differentiation of encapsulated neural stem cells. *Biomaterials* **2009**, *30* (27), 4695−4699.

(11) Li, L.; Fang, Y.; Vreeker, R.; Appelqvist, I.; Mendes, E. Reexamining the egg-box model in calcium− alginate gels with X-ray diffraction. *Biomacromolecules* **2007**, *8* (2), 464−468.

(12) Sikorski, P.; Mo, F.; Skjåk-Bræk, G.; Stokke, B. T. Evidence for egg-box-compatible interactions in calcium− alginate gels from fiber X-ray diffraction. *Biomacromolecules* **2007**, *8* (7), 2098−2103.

(13) Liu, S.; Li, H.; Tang, B.; Bi, S.; Li, L. Scaling law and microstructure of alginate hydrogel. *Carbohydr. Polym.* **2016**, *135*, 101−109.

(14) Hsiong, S. X.; Cooke, P. H.; Kong, H. J.; Fishman, M. L.; Ericsson, M.; Mooney, D. J. AFM imaging of RGD presenting

synthetic extracellular matrix using gold nanoparticles. *Macromol. Biosci.* **2008**, *8* (6), 469−477.
(15) Aston, R.; Sewell, K.; Klein, T.; Lawrie, G.; Grøndahl, L. Evaluation of the impact of freezing preparation techniques on the characterisation of alginate hydrogels by cryo-SEM. *Eur. Polym. J.* **2016**, *82*, 1−15.
(16) Zmora, S.; Glicklis, R.; Cohen, S. Tailoring the pore architecture in 3-D alginate scaffolds by controlling the freezing regime during fabrication. *Biomaterials* **2002**, *23* (20), 4087−4094.
(17) El Hariri El Nokab, M.; Lasorsa, A.; Sebakhy, K. O.; Picchioni, F.; van der Wel, P. C. Solid-state NMR spectroscopy insights for resolving different water pools in alginate hydrogels. *Food Hydrocolloids* **2022**, *127*, 107500.
(18) Müller, D. J.; Dufrene, Y. F. Atomic force microscopy as a multifunctional molecular toolbox in nanobiotechnology. *Nat. Nanotechnol.* **2008**, *3* (5), 261−269.
(19) Stylianou, A.; Kontomaris, S.-V.; Grant, C.; Alexandratou, E. Atomic force microscopy on biological materials related to pathological conditions. *Scanning* **2019**, *2019* (1), 8452851−8452925.
(20) Radić, T. M.; Svetličić, V.; Žutić, V.; Boulgaropoulos, B. Seawater at the nanoscale: marine gel imaged by atomic force microscopy. *J. Mol. Recognit.* **2011**, *24* (3), 397−405.
(21) Wang, H.; Wan, Y.; Wang, W.; Li, W.; Zhu, J. Effect of calcium ions on the III steps of self-assembly of SA investigated with atomic force microscopy. *Int. J. Food Properties* **2018**, *21* (1), 1995−2006.
(22) Li, M.; Li, H.; Li, X.; Zhu, H.; Xu, Z.; Liu, L.; Ma, J.; Zhang, M. A bioinspired alginate-gum arabic hydrogel with micro-/nanoscale structures for controlled drug release in chronic wound healing. *ACS Appl. Mater. Interfaces* **2017**, *9* (27), 22160−22175.
(23) Solbu, A. A.; Koernig, A.; Kjesbu, J. S.; Zaytseva-Zotova, D.; Sletmoen, M.; Strand, B. L. High resolution imaging of soft alginate hydrogels by atomic force microscopy. *Carbohydr. Polym.* **2022**, *276*, 118804.
(24) Decho, A. W. Imaging an alginate polymer gel matrix using atomic force microscopy. *Carbohydrate Res.* **1999**, *315* (3−4), 330−333.
(25) Nalam, P. C.; Gosvami, N. N.; Caporizzo, M. A.; Composto, R. J.; Carpick, R. W. Nano-rheology of hydrogels using direct drive force modulation atomic force microscopy. *Soft Matter* **2015**, *11* (41), 8165−8178.
(26) Engler, A. J.; Richert, L.; Wong, J. Y.; Picart, C.; Discher, D. E. Surface probe measurements of the elasticity of sectioned tissue, thin gels and polyelectrolyte multilayer films: correlations between substrate stiffness and cell adhesion. *Surface Sci.* **2004**, *570* (1−2), 142−154.
(27) Lulevich, V.; Zink, T.; Chen, H.-Y.; Liu, F.-T.; Liu, G.-y. Cell mechanics using atomic force microscopy-based single-cell compression. *Langmuir* **2006**, *22* (19), 8151−8155.
(28) Lulevich, V.; Shih, Y.-P.; Lo, S. H.; Liu, G.-y. Cell tracing dyes significantly change single cell mechanics. *J. Phys. Chem. B* **2009**, *113* (18), 6511−6519.
(29) Cleveland, J. P.; Manne, S.; Bocek, D.; Hansma, P. K. A nondestructive method for determining the spring constant of cantilevers for scanning force microscopy. *Rev. Sci. Instrum.* **1993**, *64* (2), 403−405.
(30) Hertz, H. The contact of elastic solids. *J. Reine Angew., Math* **1881**, *92*, 156−171.
(31) Yoffe, E. Modified Hertz theory for spherical indentation. *Philosophical Magazine A* **1984**, *50* (6), 813−828.
(32) Baniasadi, M.; Minary-Jolandan, M. Alginate-collagen fibril composite hydrogel. *Materials* **2015**, *8* (2), 799−814.
(33) Jejurikar, A.; Lawrie, G.; Martin, D.; Grøndahl, L. A novel strategy for preparing mechanically robust ionically cross-linked alginate hydrogels. *Biomed. Mater.* **2011**, *6* (2), 025010.
(34) Ho, S. S.; Murphy, K. C.; Binder, B. Y.; Vissers, C. B.; Leach, J. K. Increased survival and function of mesenchymal stem cell spheroids entrapped in instructive alginate hydrogels. *Stem Cells Transl. Med.* **2016**, *5* (6), 773−781.
(35) Schmitt, A.; Rödel, P.; Anamur, C.; Seeliger, C.; Imhoff, A. B.; Herbst, E.; Vogt, S.; Van Griensven, M.; Winter, G.; Engert, J. Calcium alginate gels as stem cell matrix−making paracrine stem cell activity available for enhanced healing after surgery. *PLoS One* **2015**, *10* (3), No. e0118937.
(36) Nunamaker, E. A.; Otto, K. J.; Kipke, D. R. Investigation of the material properties of alginate for the development of hydrogel repair of dura mater. *J. Mech. Behavior Biomed. Mater.* **2011**, *4* (1), 16−33.
(37) Gao, J.; Dennis, J. E.; Muzic, R. F.; Lundberg, M.; Caplan, A. I. The dynamic in vivo distribution of bone marrow-derived mesenchymal stem cells after infusion. *Cells Tissues Organs* **2001**, *169* (1), 12−20.
(38) Schrepfer, S.; Deuse, T.; Reichenspurner, H.; Fischbein, M.; Robbins, R.; Pelletier, M. Stem cell transplantation: the lung barrier. *Transplantation Proceedings*; Elsevier, 2007; pp 573−576.
(39) Hecht, H.; Srebnik, S. Structural characterization of sodium alginate and calcium alginate. *Biomacromolecules* **2016**, *17* (6), 2160−2167.
(40) He, X.; Liu, Y.; Li, H.; Li, H. Single-stranded structure of alginate and its conformation evolvement after an interaction with calcium ions as revealed by electron microscopy. *RSC Adv.* **2016**, *6* (115), 114779−114782.
(41) Leijnse, N.; Barooji, Y. F.; Arastoo, M. R.; Sønder, S. L.; Verhagen, B.; Wullkopf, L.; Erler, J. T.; Semsey, S.; Nylandsted, J.; Oddershede, L. B.; et al. Filopodia rotate and coil by actively generating twist in their actin shaft. *Nat. Commun.* **2022**, *13* (1), 1636.
(42) Mørch, Ý. A.; Donati, I.; Strand, B. L.; Skjak-Braek, G. Effect of Ca2+, Ba2+, and Sr2+ on alginate microbeads. *Biomacromolecules* **2006**, *7* (5), 1471−1480.
(43) Skjåk-Bræk, G.; Grasdalen, H.; Smidsrød, O. Inhomogeneous polysaccharide ionic gels. *Carbohydr. Polym.* **1989**, *10* (1), 31−54.
(44) Martinsen, A.; Skjåk-Bræk, G.; Smidsrød, O. Alginate as immobilization material: I. Correlation between chemical and physical properties of alginate gel beads. *Biotechnol. Bioeng.* **1989**, *33* (1), 79−89.
(45) Draget, K. I.; Taylor, C. Chemical, physical and biological properties of alginates and their biomedical implications. *Food hydrocolloids* **2011**, *25* (2), 251−256.
(46) Hernández-González, A. C.; Téllez-Jurado, L.; Rodríguez-Lorenzo, L. M. Alginate hydrogels for bone tissue engineering, from injectables to bioprinting: A review. *Carbohydr. Polym.* **2020**, *229*, 115514.
(47) Jang, J.; Seol, Y.-J.; Kim, H. J.; Kundu, J.; Kim, S. W.; Cho, D.-W. Effects of alginate hydrogel cross-linking density on mechanical and biological behaviors for tissue engineering. *J. Mech. Behavior Biomed. Mater.* **2014**, *37*, 69−77.
(48) Li, J.; Wu, Y.; He, J.; Huang, Y. A new insight to the effect of calcium concentration on gelation process and physical properties of alginate films. *J. Mater. Sci.* **2016**, *51*, 5791−5801.

https://doi.org/10.1021/acs.langmuir.4c03554
Langmuir 2024, 40, 25631−25637